LAWRENCE
LIVERMORE
NATIONAL
LABORATORY

LLNL-CONF-491472

X-ray imaging in an environment with high-neutron background on National Ignition Facility

V. A. Smalyuk, J. Ayers, P. M. Bell, J. -L. Bourgade, D. K. Bradley, J. Celeste, C. Cerjan, S. Darbon, J. Emig, B. Felker, C. Hagmann, J. Holder, N. Izumi, J. D. Kilkenny, J. Moody, K. Piston, C. Sorce, R. Tommasini

July 28, 2011

SPIE Optics + Photonics 2011
San Diego, CA, United States
August 21, 2011 through August 25, 2011

Disclaimer

X-ray imaging in an environment with high-neutron background on National Ignition Facility

V.A. Smalyuk [a], J. Ayers [a], P. M. Bell [a], J.-L. Bourgade [b], D. K. Bradley [a], J. Celeste [a], C. Cerjan [a], S. Darbon [b], J. Emig [a], B. Felker [a], C. Hagmann[a], J. Holder [a], N. Izumi [a], J. D. Kilkenny [c], J. Moody [a], K. Piston [a], A. Rousseau[b], C. Sorce [a], R. Tommasini [a]

[a]LLNL, 7000 East Ave, Livermore, USA 94550; [b]CEA, France; [c]GA, San Diego, CA

ABSTRACT

X-ray imaging instruments will operate in a harsh ionizing radiation background environment on implosion experiments at the National Ignition Facility. These backgrounds consist of mostly neutrons and gamma rays produced by inelastic scattering of neutrons. Imaging systems based on x-ray framing cameras with film and CCD's have been designed to operate in such harsh neutron-induced background environments. Some imaging components were placed inside a shielded enclosure that reduced exposures to neutrons and gamma rays. Modeling of the signal and noise of the x-ray imaging system is presented.
Keywords: x-ray imaging, neutron-induced backgrounds

1. INTRODUCTION

Time-gated, x-ray imaging [1] is an essential part of the National Ignition Campaign (NIC) [2], currently underway on the National Ignition Facility (NIF) [3].

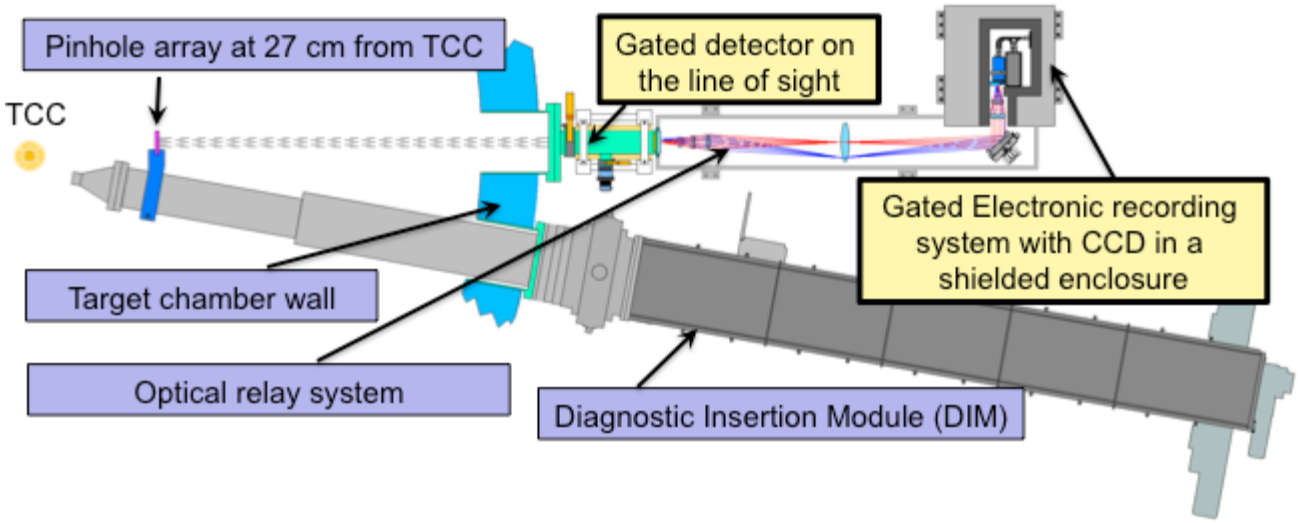

Figure 1: ARIANE consists of a 8-μm diameter pinhole array at 27 cm from TCC, a framing camera outside target chamber wall at 7 meters from TCC, optical relay system, shielded enclosure, and a gated recording system with CCD inside this enclosure for additional gating of the optical light at the output of the framing camera.

It provides temporally resolved x-ray images used for measuring shape, size, and burn history of the compressed core of imploding cryogenic deuterium-tritium (DT) capsules in Inertial Confinement Fusion (ICF) [1,2]. The symmetry and the size of the fuel during implosion are two key parameters used for optimization in tuning experiments of NIC [2,3]. The most-used x-ray imagers in ICF experiments consist of the pinhole array and a framing camera [4,5]. The pinhole array produces a large number of x-ray images on the micro-channel plate (MCP) of the framing camera. Temporal gating of the MCP allows the x-ray images to be recorded at different times. X-rays, incident on the MCP, are converted into electrons and then multiplied inside the MCP [4,5]. After leaving the MCP, the electrons are converted into visible photons in a phosphor plate. These photons are transported in a fiber-optic plate (FOP) to a detector, a CCD, or a film. The gated x-ray detectors (GXD's) can operate at DT neutron yields up to $Y_n \sim 10^{13}$ with CCD's at a standoff of 1.3 meters from Target Chamber Center (TCC). [1]. Hardened gated x-ray images (hGXI's) use film instead of CCD and can operate at DT neutron yields up to $Y_n \sim 10^{15}$ with the same standoff. [6]. Similar instruments have also been used at several other ICF facilities with moderate DT neutron yields up to $Y_n \sim 10^{13}$ when

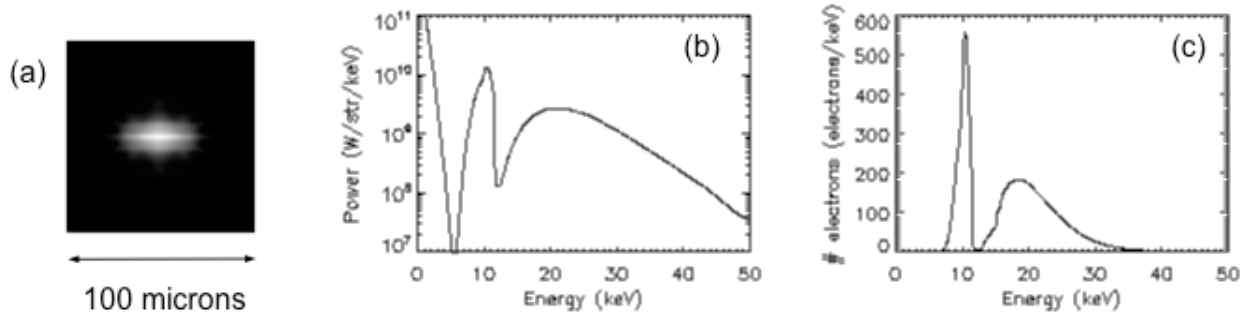

Figure 2: (a) Predicted core image at peak emission of cryogenic DT implosion with DT neutron yield of $3x10^{16}$. (b) Spectral power of x-rays emitted by a core at peak emission. (c) Number of electrons as a function of photon energy of x-rays that created them in the MCP image.

neutron-induced noise on CCD and film images and long term damage to CCD's were manageable. In the future much higher neutron yields are expected at the NIF and LMJ facilities [3] requiring imagers with increased radiation hardness. A schematic of one such gated imager is shown in Fig.1. It is called ARIANE (Active Readout In A Neutron Environment) which is designed to operate at DT neutron yields up to $Y_n \sim 10^{17}$ on NIF [7].

ARIANE consists of a pinhole array positioned at 27 cm from TCC on a DIM snout. GXD and hGXI imagers have pinholes located at closer distance of 8 cm, so the x-ray collection efficiency of the ARIANE will be about 10 times lower, compared to images used for lower yields. The framing camera will be positioned outside target chamber wall at about 7 meters from TCC, providing an object magnification of about ~25. The early version of ARIANE will use the framing camera with P-11 (blue light) phosphor [8] and film, it will be operated at DT neutron yields up to $Y_n \sim 10^{16}$. In the later version, the framing camera will use P-46 (green light) phosphor [8]. Optical light at the output of the FOP will be transported to a shielded enclosure by a F/3 optical relay system or a fiber bundle [9]. This optical light will be gated by an electronic recording system to reduce neutron-induced optical background [7]. This additional gating, together with a shielded enclosure, will allow implosion images to be recorded on CCD at DT neutron yields up to $Y_n \sim 10^{17}$. This article describes modeling of the effects of the neutron-induced backgrounds on image quality and shows the effect of the noise and resolution on the symmetry and size determination of the implosions. Section 2 describes the photometrics of implosion x-ray emission and sources of neutron-induced backgrounds. Section 3 shows the effects of these backgrounds on image quality detected by an early version of ARIANE with a framing camera with film at DT neutron yields up to $Y_n \sim 10^{16}$. Section 4 describes effects of deglitching and de-noising techniques on images detected in a shielded enclosure on CCD with a later version of ARIANE at DT neutron yields up to $Y_n \sim 10^{17}$. Section 5 summarizes the results.

2. NEUTRON-INDUCED BACKGROUNDS

Figure 2(a) shows a predicted image of the implosion core at peak x-ray emission. The image shows structure and asymmetry that is required to be measured for implosion tuning. The calculated spectral power as a function of x-ray photon energy of the core at peak emission is shown in Fig. 2(b). Reduction in calculated spectral power at ~11 keV is due to Ge K-edge absorption of the core emission in a colder Ge-doped CH shell surrounding a hot DT core. The reduction of the spectral power right below ~10 keV is due to absorption by both Ge and CH of the shell. The spectral power below ~4 keV is due emission of target outer shell. Figure 2(c) shows the number of electrons produced in the MCP image by the incident x-rays as a function of photon energy. It was calculated using ARIANE geometry, MCP quantum efficiency [10] and integrated over 80 ps, which is the temporal resolution of the framing camera. The plot shows a relative contribution of the x-rays at various photon energies in the creation of the image on a framing camera. The signal statistics are determined by number of the detected MCP electrons, rather than x-ray photons. The predicted signal at peak emission on MCP is about 0.004 "electrons"/μm^2, or 60 "electrons" per resolution element (about 5x5 μm^2 in the object plane), assuming a temporal resolution of 80 ps.

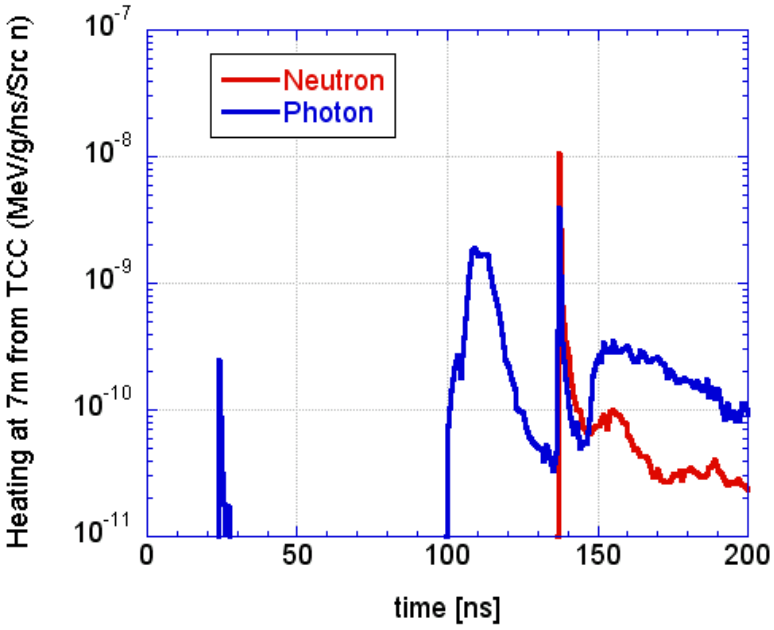

Figure 3: Calculated heating at the framing camera location at 7 m from the NIF target chamber center, for neutrons (red color) and photons (gamma rays, blue color) in the shot with DT neutron yield of $Y_n = 10^{17}$.

The neutron-induced backgrounds have two main contributions [11]: direct energy deposition by charged particles (electrons, protons, alphas, heavy ion recoils, etc.) in the film or CCD; and production of background light and signal attenuation through radiation-induced absorption in the optical image relay system [11,12]. In addition, there is cumulative damage of the CCD (increased dark current and reduced charge transfer efficiency) and glass components by long-term darkening [10]. Both optical and non-optical backgrounds are proportional to the dose of neutrons, charge particles and gammas at the detector location [11]. Figure 3 shows a heating, or a dose, at the framing camera location at 7 meters from NIF target chamber center for neutrons (red color) and photons (gamma rays) in the shot with a DT neutron yield of Yn ~ 10^{17}. The first peak at ~25 ns after the start of implosion is related to the gammas born during interactions of DT neutrons with materials of the target shell, gold hohlraum, and other material surrounding the hohlraum. At the same time, ~25 ns, x-ray emission from the implosion core will reach the framing camera and will be recorded by the imaging system. The second peak at ~100 ns, corresponds to gammas born during interactions of DT neutrons with a target chamber wall. The red peak at ~140 ns corresponds to DT neutrons.

The neutron– and gamma–induced heating after 150 ns comes from the scattered neutrons and gammas in the target bay area. The calculated integrated exposures of DT neutrons are ~$1.6x10^{10}$/cm^2 (with a dose of ~25 rads), scattered neutrons ~$2x10^{10}$/cm^2 (with a dose of ~2 rads), and gammas ~$1x10^{10}$/cm^2 (with a dose of ~5 rads). The dose from the first gamma peak at ~25 ns is about 100 times lower than the time-integrated gamma dose. At neutron yields below Yn ~ 10^{16}, the early version of ARIANE will use the framing camera with P-11 (blue light) phosphor and film. The neutron-

induced backgrounds are expected to be manageable, as shown in the next Section. However, higher yields will require modifications to imaging system to mitigate increased backgrounds. In the later ARIANE version, the framing camera will use P-46 (green light) phosphor. Optical light at the output of the FOP will be transported to a shielded enclosure by a F/3 optical relay system or a fiber bundle [9]. P-46 phosphor, although less efficient converter of electron energy to photon energy (by about 3-4 times) than P-11 phosphor, is much faster, with a measured decay time of about ~70 ns (compared to several microseconds decay time in the P-11 phosphor) [8]. Therefore, the gating of the optical output of the framing camera for about 70 ns will preclude most of the optical backgrounds (generated after ~100 ns) from reaching the detector in a shielded enclosure. In addition, the enclosure will reduce neutron flux by about two orders of magnitude, and gamma flux by about three orders of magnitude, allowing the CCD camera to record fair quality images, as shown in Section 4.

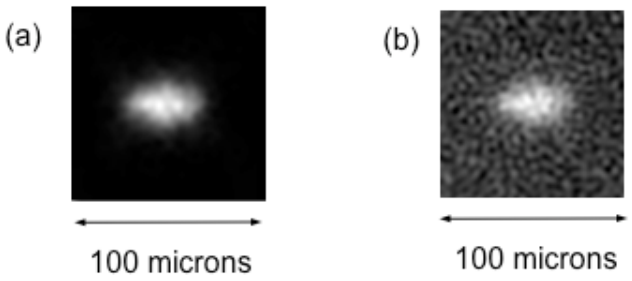

Figure 4: Image modeling for early version of ARIANE. Framing camera core images at peak emission of cryogenic DT implosion with DT neutron yield of $3x10^{16}$ without effects of neutron-induced backgrounds and film noise (a), and with effects of neutron-induced backgrounds recorded on film (b). The noise in images has been filtered out for spatial wavelengths above a resolution limit in Fourier space.

3. EFFECTS OF BACKGROUNDS ON IMAGING

Figure 4 presents modeling results of core images related to the early version of ARIANE. A simulated image of the implosion core with DT neutron yield of ~$3x10^{16}$ is shown in Fig. 2(a). It has been processed to include the effects of finite spatial resolution (~5 μm) and statistical noise of the x-rays and MCP electrons [Fig. 4(a)]. Figure 4(b) shows the same image that also includes effects of neutron-induced backgrounds and film noise.

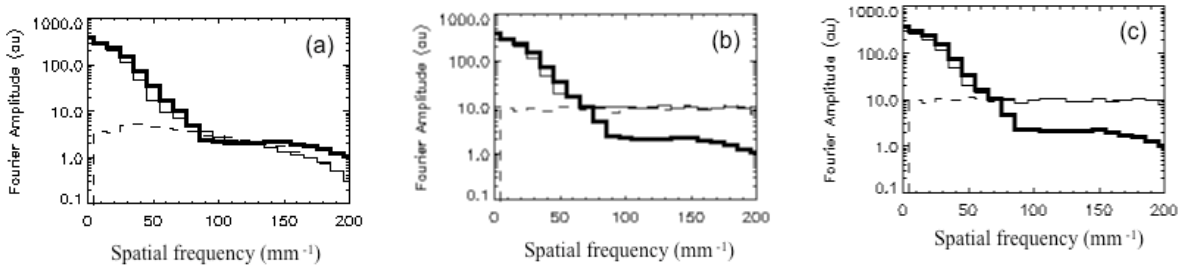

Figure 5: Fourier spectra of signal with noise (thin solid curves), noise (dashed curves), and the signal of the original image (solid thick curves) as a function of spatial frequency. Figures (a) and (b) correspond to images of early ARIANE without neutron-induced noise (a) and with neutron-induced noise on film on a shot with DT neutron yield of $3x10^{16}$ (b). Figure 5(c) corresponds to the image collected in shielded enclosure in a shot with DT neutron yield of $1x10^{17}$

The background level on Kodak TMAX-3200 film has been predicted to be ~1.6 optical density [6], corresponding to ~0.1 erg/cm^2 of optical background on film for a shot with DT neutron yield of ~$3x10^{16}$. About half of this background is due to direct interactions of neutrons with film, while the other half is due to optical backgrounds generated in the P-11 phosphor and fiber-optic plate [6]. In the modeling, the peak of the signal is twice larger than the

background, still below saturation level of the framing camera (~0.3 – 0.4 erg/cm^2 at phosphor voltage of 5 keV). Figures 5(a) and (b) show Fourier spectra of signal and noise for the images shown in Fig 4(a) and (b), respectively. The thick solid lines show Fourier spectra as a function of spatial frequency of the original image presented in Fig. 2(a), showing that modulations extend above spatial frequency above ~200 mm^{-1} (corresponding to a modulation wavelength of ~5 μm). The thin solid curves show spectra of signal with noise and dashed curves for noise only. The modulation transfer function (MTF) reduces Fourier amplitudes of the signal. When noise is added, it dominates the signal at high spatial frequencies. In fact, there is no signal above the noise at spatial frequencies above ~70 mm^{-1} (corresponding to a wavelength of ~15 μm). The noise level is higher in Fig. 5(b) when neutron-induced noise is included. Figure 5(c) shows Fourier spectra of signal and noise for the later version of ARIANE, as detected in a shielded enclosure on a CCD camera. The noise in this case is similar to the case in Fig. 5(b), but it is dominated by statistical noise of the light collected by a gated electronic system in a shielded enclosure instead of a film noise. The F/3 optical trasport system reduces signal by ~30 times during image relay. Another reduction by factor of ~3 is due to the lower efficiency of the P-46 phosphor used in the later ARIANE version, compared to the P-11 phosphor in the early version [6]. Although the optical signal can be amplified by the gated electronic system, the reduction of optical signal incident on this system increases the noise.

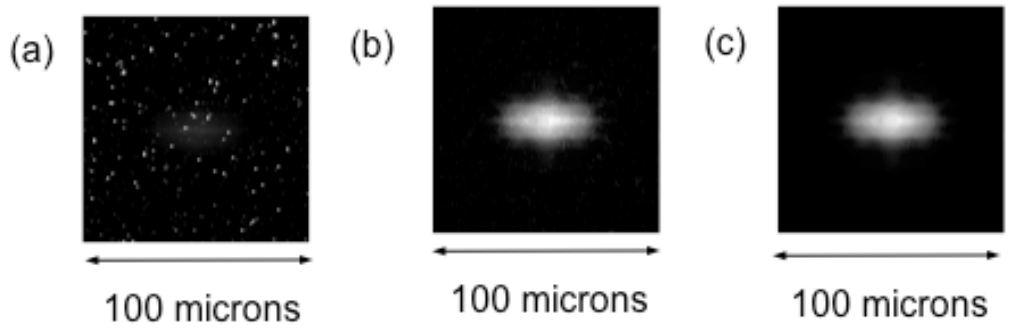

Figure 6: (a) Simulated image, shown in Fig 2(a), with added neutron-induced noise detected on CCD camera in a shot with DT neutron yield of 10^{17} in shielded enclosure. Effects of image deglitching (b) and additional de-noising techniques on noise reduction.

4. NOISE REDUCTION TECHNIQUES

The neutron-induced noises in the images detected on film and CCD camera are qualitatively different. The noise on film is essentially a uniform background, while noise on CCD consists of narrow spikes, as shown in the image on Fig. 6(a) [6,10]. Calculated neutron-induced backgrounds were added to the original image [shown Fig. 2(a)] to show expected effects of the noise on image collected in shielded enclosure on CCD camera on a shot with neutron yield of Yn ~ 10^{17} [11]. Deglitching and de-noise techniques have been developed to dramatically reduce the effects of this noise in CCD images [13]. Figure 6(b) shows an example of image deglitching, while Fig. 6(c) shows effects of both deglitching and de-noising. Figure 7 shows these effects in Fourier space. Deglitching reduces noise by ~50 times without corrupting the signal. The additional de-noising reduces the noise by additional factor of ~2, however it also reduces modulations in the signal. Image blurring due to finite system resolution has a much stronger effect on determination of image size and asymmetry than noise. For example, the original image [shown in Fig. 2(a)] radius of ~13 μm was increased to ~16 μm by the system resolution of ~5 μm. Legendre coefficients (measures of image asymmetry) in original image were 4.5 μm for L=2, and 4.0 μm for L=4. They were reduced to 4.1 μm and 1.9 μm, respectively by a 5 μm system resolution. These coefficient reductions were much larger than uncertainties in their determination due to noise in both cases of high noise [Figs. 5(b) and (c)] or lower noise [Fig. 5 (a)]. This indicates that system resolution has more effect on the determination of image size and asymmetry than noise for small size images.

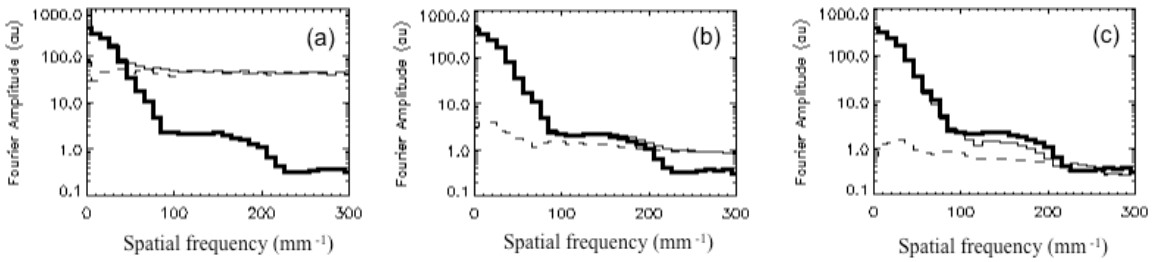

Figure 7: Fourier spectra of signal with noise (thin solid curves), noise (dashed curves), and the signal of the original image (solid thick curves) as a function of spatial frequency. The plots correspond images shown in Fig 6 recorded on CCD in shielded enclosure on a shot with DT neutron yield of $1x10^{17}$. Signal and noise spectra in images with CCD are shown in Fig. 7(a). Effects of deglitching on noise reduction are shown in Fig 7(b), while effects of additional de-noise in Fig. 7(c).

5. SUMMARY

The effects of neutron-induced backgrounds were described in gated imaging systems for inertial confinement fusion (ICF). Backgrounds in shots with DT neutron yields up to $Y_n \sim 10^{17}$ consist of mostly neutrons and gamma rays produced by inelastic scattering of neutrons as well as optical backgrounds in optical relay parts of the imaging systems. Imaging systems based on x-ray framing cameras with film and CCD's have been designed to operate in such harsh neutron-induced background environments. The early version of ARIANE will use a framing camera with P-11 (blue light) phosphor and film. It will be operated at DT neutron yields up to $Y_n \sim 10^{16}$. In the later version, the framing camera will use a P-46 (green light) phosphor. The optical light at the output of the FOP will be transported to a shielded enclosure by a F/3 optical relay system or a fiber bundle. This optical light will be gated by an electronic recording system to reduce neutron-induced optical background. This additional gating, together with a shielded enclosure, will allow implosion images to be recorded on CCD at DT neutron yields up to $Y_n \sim 10^{17}$.

ACKNOWLEDGEMENTS

Lawrence Livermore National Laboratory is operated by Lawrence Livermore National Security, LLC, for the U.S. Department of Energy, National Nuclear Security Administration under Contract No. DE-AC52-07NA27344.

REFERENCES

[1] G.A. Kyrala, S. Dixit, S. Glenzer, D. Kalantar *et al.,* Rev. Sci. Instrum. **81**, 10E316 (2010).
[2] G. H. Miller *et al.,* Nucl. Fusion **44**, S228 (2004).
[3] E. I. Moses *et al.,* Phys. Plasmas **16**, 041006 (2009).
[4] D.K. Bradley *et al.,* Rev. Sci. Instrum. **66**, 716 (1995).
[5] C. J. Pawley and A. V. Deniz, Rev. Sci. Instrum. **71**, 1286 (2000).
[6] N. Izumi, C. Hagmann, G. Stone *et al.,* Rev. Sci. Instrum. **81**, 10E515 (2010).
[7] P.M. Bell, D.K. Bradley, J.D. Kilkenny *et al.,* Rev. Sci. Instrum. **81**, 10E540 (2010).
[8] N. Izumi *et al.,* this proceedings.
[9] Schott North America, 122 Charlton St., Southbridge, MA 01550.
[10] B. L. Henke, J. P. Knauer, and K. Premaratne, J. Appl. Phys. **52**, 1509 (1981).
[11] C. Hagmann, N. Izumi, P. Bell *et al.,* Rev. Sci. Instrum. **81**, 10E514 (2010).
[12] E.J. Friebele, G.H. Sigel, Jr. and M.E. Gingerich, IEEE TNS 25, 1261 (1978).
[13] R. Tommasini, private communication.